Proceedings of the ASME 2018
Dynamic Systems and Control Conference
DSCC2018
September 30-October 3, 2018, Atlanta, Georgia, USA

DSCC2018-9089

Wide-band Loop Shaping for Modulation of Energy Transmission in Nonminimum-phase Systems

Tianyu Jiang
Dept. of Mechanical Engineering
University of Connecticut
Storrs, Connecticut, 06269
Email: tianyu.jiang@uconn.edu

Jiong Tang
Dept. of Mechanical Engineering
University of Connecticut
Storrs, Connecticut, 06269
Email: jiong.tang@uconn.edu

Xu Chen
Dept. of Mechanical Engineering
University of Connecticut
Storrs, Connecticut, 06269
Email: xchen@uconn.edu

ABSTRACT

Modulating the closed-loop transmission of energy in a wide frequency band without sacrificing overall system performance is a fundamental issue in a wide range of applications from precision control, active noise cancellation, to energy guiding. This paper introduces a loop-shaping approach to create such wide-band closed-loop behaviors, with a particular focus on systems with nonminimum-phase zeros. Pioneering an integration of the interpolation theory with a model-based parameterization of the closed loop, the work proposes a filter design that matches the inverse plant dynamics locally and creates a framework to shape energy transmission with user defined performance metrics in the frequency domain. Application to laser-based powder bed fusion additive manufacturing validates the feasibility to compensate wide-band vibrations and to flexibly control system performance at other frequencies.

1 INTRODUCTION

Active and flexible shaping of dynamic system responses is key for modulating input-to-output energy flows. For example, adaptive disturbance attenuation minimizes the energy of position error and achieves precision motion control in nm-scale in a modern hard disk drive (HDD) [1, 2]; in modern headphones, active acoustic noise cancellation reduces acoustic energy transmission from the environment to human ears [3]; wave guiding applications, on the other hand, minimizes loss of energy by restricting wave expansion to one dimension or two [4].

As a fundamental element of modulating energy transmission, feedback loop shaping in the frequency domain has attracted extensive research attention. Based on the target energy distribution, relevant control algorithms can be generally classified into two categories: narrow- and wide-band loop shaping. In the first category, the input energy concentrates at one or several frequencies. Based on such characteristics, peak filter [5, 6], repetitive control [7, 8], adaptive notch filter [9, 10], and narrow-band disturbance observer (DOB) [1, 11, 12] generate deep but narrow notches in the closed-loop error-rejection functions at frequencies where the input energy (disturbance) dominates. For wide-band loop shaping, the input energy spans over wide peaks in the spectrum map. A narrow notch cannot provide sufficient attenuation to such inputs; yet a wide notch tends to cause undesired amplification at other frequencies (the fundamental waterbed effect in feedback controls [13]). In view of such challenges, [14] proposed to detune the notch depth and place fixed zeros according to the performance criterion; [2] utilized an online adaptation algorithm to estimate both frequency and notch width for optimal loop shaping design.

In this paper, we propose a new control scheme for wide-band loop shaping for stable but nonminimum-phase systems. Compared with previous algorithms such as the DOB, this wide-band *forward model selective disturbance observer* (FMSDOB) avoids direct inversion of the plant model, thereby offering freedom and flexibility of loop shaping for nonminimum-phase systems. Compared to other loop-shaping designs, the proposed algorithm inherits benefits of DOB design regarding design intuition and strong performance [12,14]. By designing an FIR (finite impulse response) filter that matches both the plant frequency response and high-order dynamics locally, this scheme creates wide notches in the closed-loop sensitivity function. By integrating a cascaded filtering design into the Youla-Kucera (YK) parameterization, the algorithm directly controls energy amplification at other frequencies. Verification is performed by simulation on a two-axis galvo scanner in selective laser sintering additive manufacturing.

The remainder of this paper is organized as follows. Section

2 reviews the algorithmic foundation of the proposed method and its connection to our previous work on narrow-band loop shaping; Section 3 provides the main results of wide-band loop shaping design, following which Section 4 presents the supporting simulation results, and finally, Section 5 concludes this paper.

Notations: Throughout the paper, the calligraphic $\mathscr{S}$ and $\mathscr{R}$ denote, respectively, the set of stable proper rational transfer functions, and the set of proper rational transfer functions. When a linear time invariant (LTI) plant P is stabilized by an LTI controller C (in a negative feedback loop), $S(\triangleq 1/(1+PC))$ and $T(\triangleq PC/(1+PC))$ denote, respectively, the sensitivity function[1] and the complementary sensitivity function. The calligraphic $\Re$ and $\Im$ denote, respectively, the real and imaginary part of a complex number.

2 REVIEW OF RELEVANT LITERATURE

2.1 Review of Youla-Kucera parameterization

Theorem 1. *(YK Parameterization [15, 16]). If an SISO plant $P = N/D$ can be stabilized by a negative-feedback controller $C = X/Y$, with (N,D) and (X,Y) being coprime factorizations over $\mathscr{S}$, then any stabilizing feedback controller of P can be parameterized as*

$$C_{all} = \frac{X+DQ}{Y-NQ} : \; Q \in \mathscr{S},\; Y(\infty) - N(\infty)Q(\infty) \neq 0.$$

Here, (N,D) is called a coprime factorization of $P \in \mathscr{R}$ over $\mathscr{S}$ if: (i) $P = ND^{-1}$, (ii) $N(\in \mathscr{S})$ and $D(\in \mathscr{S})$ are coprime transfer functions, and (iii) $D^{-1} \in \mathscr{R}$.

A main advantage of YK Parameterization is that it renders the sensitivity function of the closed loop (i.e., the error rejection function of the feedback system) to:

$$\tilde{S} = \frac{1}{1+PC_{all}} = \frac{1}{1+PC}\left[1 - \frac{N}{Y}Q\right], \tag{1}$$

which is decoupled into the product of the baseline sensitivity $1/(1+PC)$ and the add-on affine module $1-NQ/Y$. Because stability is assured under the controller parameterization, designers can now focus on the add-on module (which depends affinly on Q) to achieve desired performance features.

2.2 Forward Model Selective Disturbance Observer

When P and C are stable, one can factorize them in Theorem 1 as $N(z) = P(z)$, $D(z) = 1$, $X(z) = C(z)$, $Y(z) = 1$. (These are special plant-controller pairs that often arise in mechatronic systems.) Then

$$C_{all} = \frac{C(z)+Q(z)}{1-P(z)Q(z)},\; Q(z) \in \mathscr{S}$$

parameterizes all stabilizing controllers for $P(z)$, and the new sensitivity function is

$$S = \frac{1}{1+P(z)C(z)}(1-P(z)Q(z)) \triangleq S_0(z)(1-P(z)Q(z)). \tag{2}$$

The factorization above renders the add-on module in (1) to $1-P(z)Q(z)$. This parameterization has made the added module simple and do not depend on baseline controller $C(z)$. Certainly, from the viewpoint of implementation, a perfect plant model is unrealistic in practice. In this sense, instead of $P(z)$, a nominal model of the plant $\hat{P}(z)$ is used to formulate the YK parameterization, which gives the new stabilizing controller and sensitivity function

$$\tilde{C}_{all} = \frac{C(z)+Q(z)}{1-\hat{P}(z)Q(z)},\; Q(z) \in \mathscr{S}$$
$$\tilde{S} = \frac{1}{1+P(z)C(z)+(P(z)-\hat{P}(z))Q(z)}(1-\hat{P}(z)Q(z)). \tag{3}$$

At frequencies where $P(e^{j\omega}) = \hat{P}(e^{j\omega})$, i.e. where the nominal model is accurate, (3) gives

$$\tilde{S} = \frac{1}{1+P(e^{j\omega})C(e^{j\omega})}(1-P(e^{j\omega})Q(e^{j\omega})),$$

i.e. the decoupling of sensitivity in (2) remains valid in the frequency domain. Loop shaping and energy transmission modulation then translate to designing $1-P(e^{j\omega})Q(e^{j\omega}) = 0$, which gives $\tilde{S}(e^{j\omega}) = 0$. One intuitive design is thus to make $Q(z) = P^{-1}(z)$, namely, direct inversion of the plant model. However, when the plant contains unstable zero(s) or is strictly proper, a direct inversion will introduce instability or non-properness to the closed loop. In our previous work [17, 18], we proposed a pointwise inverse design to overcome these fundamental challenges. The main result is provided in the following proposition.

Proposition 2. *Let $Q(z) = b_0 + \sum_{l=1}^{m} b_l z^{-l}$, with*

$$\begin{bmatrix} b_0 \\ \vdots \\ b_m \end{bmatrix} = \begin{bmatrix} 1 & \cos\omega_1 & \dots & \cos m\omega_1 \\ 0 & \sin\omega_1 & \dots & \sin m\omega_1 \\ \vdots & & & \vdots \\ \vdots & & & \vdots \\ 1 & \cos\omega_n & \dots & \cos m\omega_n \\ 0 & \sin\omega_n & \dots & \sin m\omega_n \end{bmatrix}^{-1} \begin{bmatrix} \frac{\Re P(e^{j\omega_1})}{|P(e^{j\omega_1})|^2} \\ \frac{\Im P(e^{j\omega_1})}{|P(e^{j\omega_1})|^2} \\ \vdots \\ \vdots \\ \frac{\Re P(e^{j\omega_n})}{|P(e^{j\omega_n})|^2} \\ \frac{\Im P(e^{j\omega_n})}{|P(e^{j\omega_n})|^2} \end{bmatrix}, \tag{4}$$

where $m = 2n-1$. Then

$$Q(e^{j\omega_i})P(e^{j\omega_i}) = 1,\; \forall i = 1,2,\dots,n.$$

[1] The transfer function from the output disturbance to the plant output.

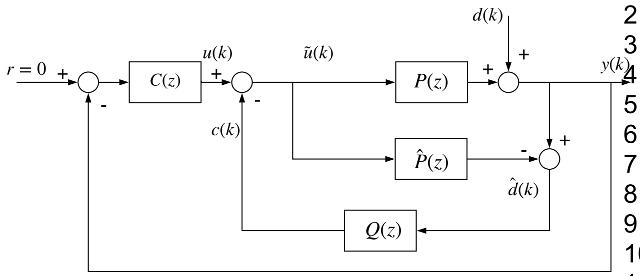

FIGURE 1. PROPOSED FORWARD MODEL SELECTIVE DISTURBANCE OBSERVER SCHEME.

Proof. See [18]. □

By focusing on the local inversion of $P(e^{j\omega})$, Proposition 2 relaxes the requirement of a stable plant inversion. Proof of the closed-loop stability and robustness of the proposed scheme is provided in [18]. Briefly speaking, since the forward model based controller is branched out of the YK parameterization, nominal stability follows directly. On the other hand, at frequencies where there are large model uncertainties and mismatches, high-performance control intrinsically has to be sacrificed for robustness based on robust control theory. It is not difficult to make $Q(e^{j\omega})$ small at these frequencies to keep the influence of the mismatch element $(P(z)-\hat{P}(z))Q(z)$ small in (3).

Fig. 1 shows a realization of the scheme discussed above. We have the following relevant signals and transfer functions:

$P(z)$ and $\hat{P}(z)$: the plant and its identified model;
$C(z)$: a baseline controller designed to provide a robustly stable closed loop;
$d(k)$ and $\hat{d}(k)$: the actual (not measurable) disturbance and its online estimate;
$\tilde{u}(k)$ and $u(k)$: the control command with and without the compensation signal;
$y(k)$: measured residual error;
$c(k)$: the compensation signal that asymptotically rejects the disturbance $d(k)$.

Remark 3. We assume that the magnitude of $P(e^{j\omega})$ is not zero at the target frequencies (otherwise, disturbances are directly rejected by the plant).

Remark 4. By block diagram analysis, if $P(e^{j\omega_i})=\hat{P}(e^{j\omega_i})$, one can show that when $r(k)=0$ and $P(e^{j\omega_i})Q(e^{j\omega_i})=1$, $P(z)\tilde{u}(k)$ approximates $-d(k)$ at ω_i (hence canceling the disturbance).

We will use this intuition of disturbance estimation for controller tuning.

3 PROPOSED WIDE-BAND LOOP SHAPING FOR NONMINIMUM-PHASE SYSTEMS

Compared with single-frequency excitation, wide-band signals (see, e.g., Fig. 2) induce widely spanned spectral peaks. For such cases, pointwise inversion of the plant frequency response alone will not generate satisfying loop-shaping result.

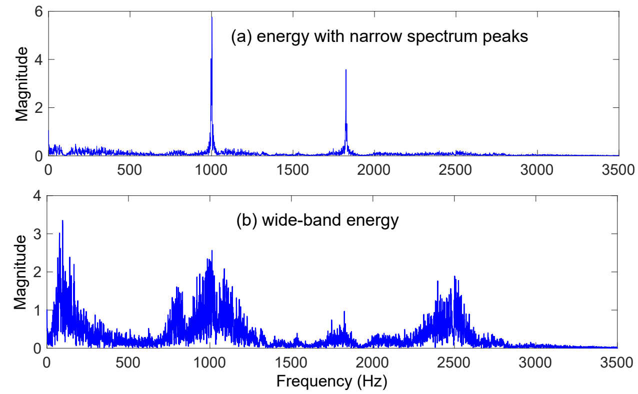

Fig. 1. Examples of HDD disturbance spectra.

FIGURE 2. EXAMPLE OF WIDE-BAND DISTURBANCE SPECTRUM [2].

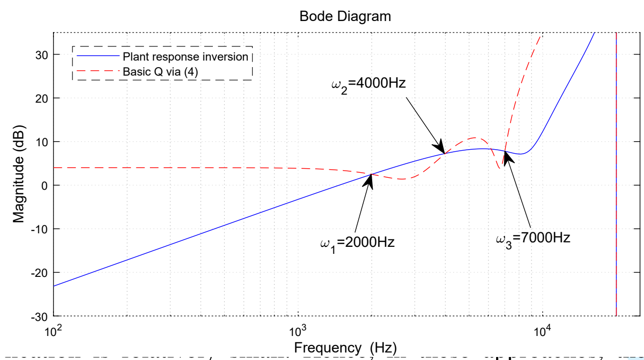

FIGURE 3. COMPARISON OF THE INVERSE MAGNITUDE RESPONSE OF A PLANT AND FREQUENCY RESPONSE OF Q FILTER GENERATED BY (4).

This can be seen in Fig. 3, which compares the inverse magnitude response of a plant and corresponding $Q(e^{j\omega})$ designed from (4). Note the different slope rates of these two lines at the target frequencies (2000Hz, 4000Hz, 7000Hz). As the frequency deviates from these points, the response of add-on module $1-P(e^{j\omega})Q(e^{j\omega})$ can easily fall out of desired performance threshold. In this section, we propose an augmented Q filter design so that both $1-P(e^{j\omega})Q(e^{j\omega})$ and its first-order derivative are zero at the center of each frequency band. The result is that the frequency response of Q filter matches the inverse response of the plant not only at but also around the target frequencies, which introduces wide loop-shaping notches in the frequency response of the add-on module $1-P(e^{j\omega})Q(e^{j\omega})$.

Proposition 5. *Let $\omega_i \in (0,\pi)$, $i=1,2,\ldots,n$ be center frequencies of the target loop-shaping regions, (N,D) be a coprime factorization of P such that $P=N/D$, where $N=\sum_{u=0}^{p}c_u z^{-u}$ and $D=z^q+\sum_{v=0}^{q}a_v z^{-v}$. Design*

$$Q(z)=b_0+\sum_{l=1}^{m}b_l z^{-l} \quad (5)$$

...adaptation focuses mainly on finding the optimal attenuation frequencies. Yet for multiple wide-band disturbance attenuation, such undesired amplifications are much more dangerous, and should be systematically considered in controller design to avoid deterioration of the overall performance.

In view of the needs and challenges, an adaptive loop shaping scheme is proposed in this paper for multiple wide-band disturbance attenuation. By considering adaptations w.r.t. not only the attenuation frequencies but also the attenuation widths, this scheme automatically tunes for the optimal controller parameters that offer better overall performance. Such a two-degree-of-freedom (2-DOF) adaptation allows an optimal allocation of control efforts over all frequencies. It balances the preferred disturbance attenuation and undesired amplification with minimum position errors. As an extension to our previous work [18]–[20], [24]–[26], this paper contributes in three aspects:[1] (i) the adaptive controller design covers both single and dual-stage HDDs; (ii) wide-band disturbances with the important extension to multiple spectral peaks are addressed; and (iii) experimental verification on a Voice-Coil-Driven Flexible Positioner (VCFP) system is performed.

The remainder of the paper is organized as follows. Section II presents the proposed adaptive control structure for both single and dual-stage HDDs. Section III discusses the performance-oriented Q filter design with tunable passband widths. In Section IV, the 2-DOF parameter adaptation algorithms are formulated. Stability analysis is given in Section V, followed by the experimental results on a VCFP system in Section VI. Finally, Section VII concludes the paper.

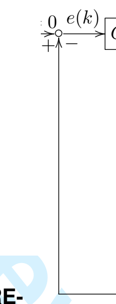

Fig. 2. The ...

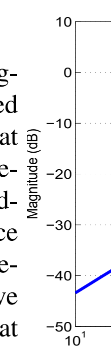

Fig. 3. Typic...

with $m = 4n-1$ and

$$\begin{bmatrix} b_0 \\ \vdots \\ b_m \end{bmatrix} = \begin{bmatrix} 1 & \cos\omega_1 & \cos 2\omega_1 & \dots & \cos m\omega_1 \\ 0 & \sin\omega_1 & \sin 2\omega_1 & \dots & \sin m\omega_1 \\ \vdots & & & & \vdots \\ 1 & \cos\omega_n & \cos 2\omega_n & \dots & \cos m\omega_n \\ 0 & \sin\omega_n & \sin 2\omega_n & \dots & \sin m\omega_n \\ \hline 0 & \cos\omega_1 & 2\cos 2\omega_1 & \dots & m\cos m\omega_1 \\ 0 & \sin\omega_1 & 2\sin 2\omega_1 & \dots & m\sin m\omega_1 \\ \vdots & & & & \vdots \\ 0 & \cos\omega_n & 2\cos 2\omega_n & \dots & m\cos m\omega_n \\ 0 & \sin\omega_n & 2\sin 2\omega_n & \dots & m\sin m\omega_n \end{bmatrix}^{-1} \begin{bmatrix} \frac{\Re P(e^{j\omega_1})}{|P(e^{j\omega_1})|^2} \\ \frac{\Im P(e^{j\omega_1})}{|P(e^{j\omega_1})|^2} \\ \vdots \\ \frac{\Re P(e^{j\omega_n})}{|P(e^{j\omega_n})|^2} \\ \frac{\Im P(e^{j\omega_n})}{|P(e^{j\omega_n})|^2} \\ \hline -\Re H(e^{j\omega_1}) \\ \Im H(e^{j\omega_1}) \\ \vdots \\ -\Re H(e^{j\omega_n}) \\ \Im H(e^{j\omega_n}) \end{bmatrix}, \tag{6}$$

where

$$H(e^{j\omega}) = \frac{(qe^{jq\omega} + \sum_{v=1}^{q-1} va_v e^{jv\omega})N(e^{j\omega}) - (\sum_{u=1}^{p} uc_u e^{ju\omega})D(e^{j\omega})}{N^2(e^{j\omega})},$$

then

$$\begin{cases} 1 - P(e^{j\omega_i})Q(e^{j\omega_i}) & = 0 \\ \frac{\mathrm{d}}{\mathrm{d}\omega}(1 - P(e^{j\omega})Q(e^{j\omega}))\,|_{\omega=\omega_i} & = 0. \end{cases} \tag{7}$$

Proof. We first derive the conditions for the first equation in (7). When $P(e^{j\omega_i}) \neq 0$, this can be rewritten as

$$Q(e^{j\omega_i}) = \frac{1}{P(e^{j\omega_i})} = \frac{\overline{P(e^{j\omega_i})}}{|P(e^{j\omega_i})|^2},$$

i.e.

$$\begin{cases} \Im Q(e^{j\omega_i}) = -\frac{\Im P(e^{j\omega_i})}{|P(e^{j\omega_i})|^2} \\ \Re Q(e^{j\omega_i}) = \frac{\Re P(e^{j\omega_i})}{|P(e^{j\omega_i})|^2} \end{cases}, \ i = 1, 2, \dots, n. \tag{8}$$

Given $Q(z) = b_0 + \sum_{l=1}^{m} b_l z^{-l}$, (8) becomes

$$b_0 + \sum_{l=1}^{m} b_l \cos l\omega_i = \frac{\Re P(e^{j\omega_i})}{|P(e^{j\omega_i})|^2}$$
$$\sum_{l=1}^{m} b_l \sin l\omega_i = \frac{\Im P(e^{j\omega_i})}{|P(e^{j\omega_i})|^2}.$$

In matrix form, these conditions are shown in the upper section of the right hand side of (6).

Now we prove the conditions of the second equation in (7), which is equivalent to

$$(\frac{\mathrm{d}P(e^{j\omega})}{\mathrm{d}\omega}Q(e^{j\omega}) + \frac{\mathrm{d}Q(e^{j\omega})}{\mathrm{d}\omega}P(e^{j\omega}))|_{\omega=\omega_i} = 0.$$

When $1 - P(e^{j\omega_i})Q(e^{j\omega_i}) = 0$ and $P(e^{j\omega_i}) \neq 0$, this becomes

$$(\frac{\mathrm{d}P(e^{j\omega})}{\mathrm{d}\omega}\frac{1}{P(e^{j\omega})} + \frac{\mathrm{d}Q(e^{j\omega})}{\mathrm{d}\omega}P(e^{j\omega}))\,|_{\omega=\omega_i} = 0,$$

i.e.

$$\frac{\mathrm{d}Q(e^{j\omega})}{\mathrm{d}\omega}\,|_{\omega=\omega_i} = -\frac{1}{P^2(e^{j\omega})}\frac{\mathrm{d}P(e^{j\omega})}{\mathrm{d}\omega}\,|_{\omega=\omega_i} = \frac{\mathrm{d}}{\mathrm{d}\omega}\frac{1}{P(e^{j\omega})}\,|_{\omega=\omega_i}. \tag{9}$$

Given again $Q(z) = b_0 + \sum_{l=1}^{m} b_l z^{-l}$, the left hand side of (9) is

$$\frac{\mathrm{d}Q(e^{j\omega})}{\mathrm{d}\omega}\,|_{\omega=\omega_i} = -\sum_{l=1}^{m} b_l l \sin l\omega_i - j\sum_{l=1}^{m} b_l l \cos l\omega_i. \tag{10}$$

Given the coprime factorization of $P = ND^{-1}$, the right hand side of (9) becomes

$$\begin{aligned} &\frac{\mathrm{d}}{\mathrm{d}\omega}\frac{1}{P(e^{j\omega})}\,|_{\omega=\omega_i} \\ =&\frac{\mathrm{d}}{\mathrm{d}z}\frac{1}{P(z)}\frac{\mathrm{d}z}{\mathrm{d}\omega}\,|_{z=e^{j\omega_i}} \\ =&\frac{\mathrm{d}}{\mathrm{d}z}\frac{D(z)}{N(z)}\frac{\mathrm{d}z}{\mathrm{d}\omega}\,|_{z=e^{j\omega_i}} \\ =&j\frac{\frac{\mathrm{d}}{\mathrm{d}z}D(z)N(z) - \frac{\mathrm{d}}{\mathrm{d}z}N(z)D(z)}{N^2(z)}z\,|_{z=e^{j\omega_i}} \\ =&j\frac{(qz^q + \sum_{v=1}^{q-1} va_v z^v)N(z) - (\sum_{u=1}^{p} uc_u z^u)D(z)}{N^2(z)}|_{z=e^{j\omega_i}} \\ =&jH(e^{j\omega_i}). \end{aligned} \tag{11}$$

Matching the real and imaginary parts of (10) and (11) for $i = 1, 2, \dots, n$ gives the lower section of (6).

There are $4n$ linear independent equations in (6), the minimum order for Q is $m = 4n-1$. □

Corollary 6. *If (7) is true, then*

$$\frac{\mathrm{d}}{\mathrm{d}\omega}\left|1 - P(e^{j\omega})Q(e^{j\omega})\right|\,|_{\omega=\omega_i} = 0.$$

Proof. Assume that $1 - P(e^{j\omega})Q(e^{j\omega}) = A(\omega)e^{j\theta(\omega)}$, where $A(\omega)$ and $\theta(\omega)$ are the magnitude and frequency responses, respectively. Then

$$\frac{\mathrm{d}}{\mathrm{d}\omega}(1 - P(e^{j\omega})Q(e^{j\omega})) = \frac{\mathrm{d}A(\omega)}{\mathrm{d}\omega}e^{j\theta(\omega)} + jA(\omega)\frac{\mathrm{d}\theta(\omega)}{\mathrm{d}\omega}e^{j\theta(\omega)} = 0.$$

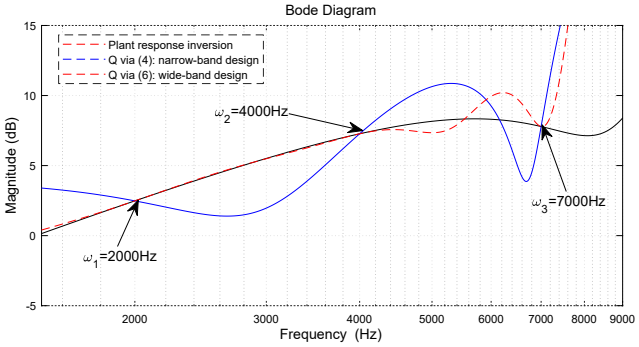

FIGURE 4. COMPARISON OF MAGNITUDE RESPONSE FOR DIFFERENT Q FILTER DESIGNS.

Note that $A(\omega_i) = 0$. The above equation then gives

$$\frac{\mathrm{d}}{\mathrm{d}\omega}(1 - P(e^{j\omega})Q(e^{j\omega}))\,|_{\omega=\omega_i} = \frac{\mathrm{d}A(\omega)}{\mathrm{d}\omega} e^{j\theta(\omega)}\,|_{\omega=\omega_i} = 0,$$

which is equivalent to

$$\frac{\mathrm{d}A(\omega)}{\mathrm{d}\omega} = \frac{\mathrm{d}}{\mathrm{d}\omega}\left|1 - P(e^{j\omega})Q(e^{j\omega})\right|\,|_{\omega=\omega_i} = 0.$$

□

Consider again the case in Fig. 3. The frequency response of the proposed $Q(e^{j\omega})$ from (6) is added, which is shown in Fig. 4. Compared with the basic solution (4), the magnitude response of the filter that incorporates higher-order plant dynamics is seen to match the inverse magnitude response of $P(z)$ within a large band around the target frequencies.

The magnitude response of $1 - PQ$ in Fig. 5 further illustrates the benefit of (6) for wide-band loop shaping. It can be seen that the new filter design gives a wider notch shape at all three target frequencies. A zoom-in view of the magnitude response of $1 - PQ$ shows that the proposed wide-band design indeed achieves zero derivative (which is guaranteed by Corollary 6) at the target frequencies, creating lower magnitudes at the frequency regions centered around these points.

For implementation, one can calculate $H(e^{j\omega})$ based on the analytic transfer function, or directly calculate the derivative of the inverse frequency response on the right hand side of (9) by using measured frequency responses of $P(e^{j\omega})$.

The proposed FIR filter achieves desired energy transmission modulation at ω_i. Yet, because there is no constraint on the overall magnitude, this basic solution tends to induce undesired amplification when $\omega \neq \omega_i$, especially at frequencies far away from the target frequency. Such waterbed effect is particularly severe and dangerous in wide-band loop-shaping design. Meanwhile, at frequencies where there are large model uncertainties and mismatches, high-performance control intrinsically has to be sacrificed for robustness based on robust control theory. Thus, the proposed implementation form is to incorporate special bandpass characteristics to maintain the magnitude of

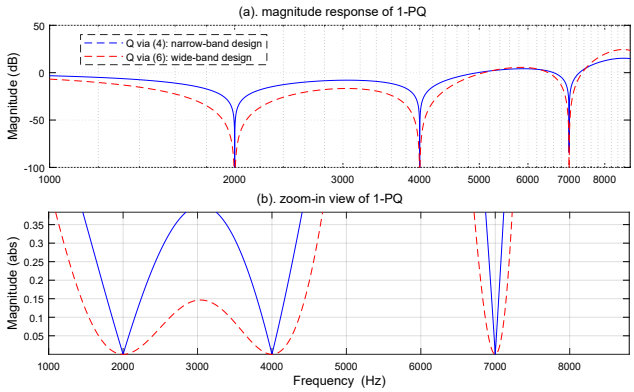

FIGURE 5. MAGNITUDE RESPONSE OF 1-PQ FOR DIFFERENT Q DESIGNS.

$Q(e^{j\omega})$ small when $\omega \neq \omega_i$. More specifically, we propose the following lattice-structure [19] bandpass filter

$$Q_{BP}(z) = 1 - \frac{1}{2^n}\prod_{i=1}^{n}\frac{(1+k_{2,i})(1+2k_{1,i}z^{-1}+z^{-2})}{1+k_{1,i}(1+k_{2,i})z^{-1}+k_{2,i}z^{-2}}, \qquad (12)$$

where $k_{1,i} = -\cos\omega_i$ and $k_{2,i} = [1 - \tan(B_{w,i}/2)]/[1 + \tan(B_{w,i}/2)]$, $B_{w,i}$ (in radian) is the 3-dB bandwidth of $Q_{BP}(z)$ centered around ω_i. It can be shown that $Q_{BP}(e^{j\omega_i}) = 1, \forall i = 1, 2, \ldots, n$. Applying (12) to (5) gives

$$Q(z) = Q_{BP}(z)(b_0 + \sum_{l=1}^{m} b_l z^{-l}), \qquad (13)$$

which not only maintains the desired wide-band loop shape, but also blocks noises in $d(k)$ outside the target frequency ranges.

4 SIMULATION VERIFICATION

The proposed algorithm is verified by simulation on a two-axis galvo scanner in selective laser sintering additive manufacturing. The identified plant transfer function is

$$\hat{P}(z) = \frac{0.0282z^2 + 0.1504z + 0.1146}{z^4 - 1.3190z^3 + 0.929z^2 - 0.6073z - 0.0035}, \qquad (14)$$

where the sampling time $T_s = 0.025$ms. A figure that shows the frequency response of (14) compared with the measured response is provided in [18]. Note that this is a nonminimum-phase system with an unstable zero at $z = -4.419$. A vendor-integrated baseline controller is already embedded in the plant. We thus set $C(z) = 1$ in Fig. 1. The magnitude response of the baseline sensitivity function is provided in Fig. 6. The system has a bandwidth around 1000Hz.

Fig. 7 shows spectrum of the wide-band disturbance used in the simulation[2]. The vibrations contain three major wide-band

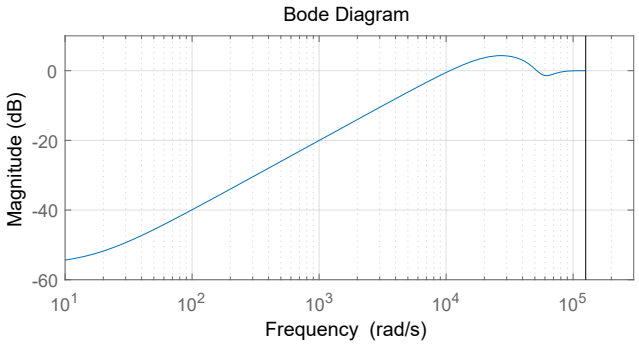

FIGURE 6. MAGNITUDE RESPONSE OF BASELINE SENSITIVITY FUNCTION.

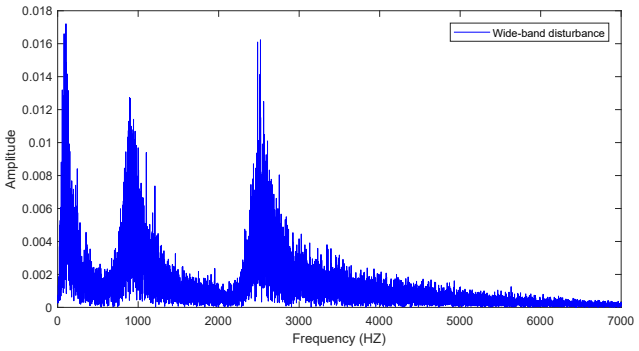

FIGURE 7. WIDE-BAND DISTURBANCE IN SIMULATION.

peaks centered around 100Hz, 900Hz, and 2500Hz.

The baseline sensitivity function already attenuates the low frequency signal. Thus, in the Q filter design, we only focus on the higher bands (900Hz and 2500Hz). Fig. 8 shows magnitude responses of the Q filter and $1-PQ$. As expected, two wide attenuation notches are located at the target frequencies in the upper plot. To mitigate the large amplification in high frequency region due to waterbed effect, the red dashed line shows the result of applying the lattice-structure bandpass filter in (12). The corresponding performance in time and frequency domain is shown in Fig. 9 and Fig. 10, respectively. It can be seen that the low frequency band is rejected in both plots thanks to the baseline sensitivity function (recall Fig. 6). However, as the input energy frequency increases, baseline sensitivity function is not powerful enough anymore. On the other hand, the proposed scheme is able to effectively attenuate the large spectral peaks.

5 CONCLUSION AND FUTURE WORK

In this paper, a wide-band loop shaping scheme for modulating energy transmission in a feedback system is introduced. This algorithm is constructed by designing a pointwise model inversion filter. The proposed scheme avoids explicit plant inversions and is particularly useful for nonminimum-phase systems or when a stable plant inversion is prohibitively expensive over the full frequency range. Simulation on a galvo scanner platform

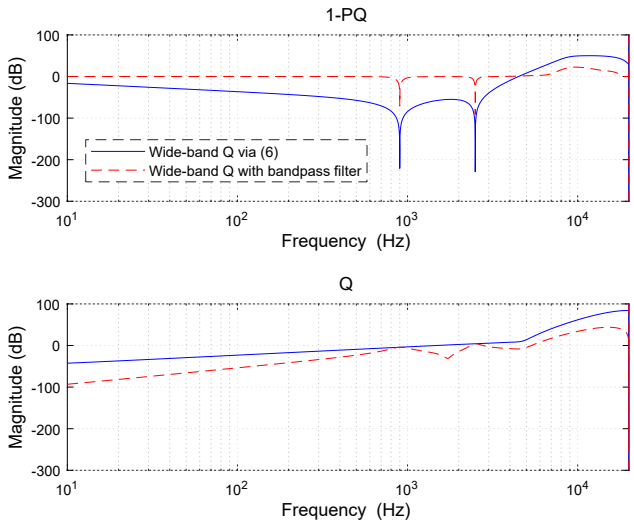

FIGURE 8. MAGNITUDE RESPONSES OF THE WIDE-BAND Q FILTER AND $1-PQ$.

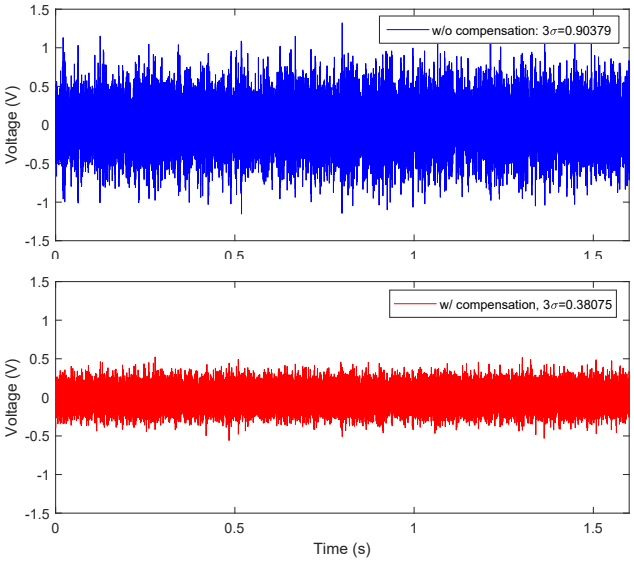

FIGURE 9. TIME SERIES COMPARISON WITH AND WITHOUT THE PROPOSED WIDE-BAND Q COMPENSATOR.

in selective laser sintering shows significant performance gains for attenuating multiple wide-band energy transmission. The result is achieved by utilizing the first-order derivative of plant dynamics response for the loop-shaping filter design. Experimentation on actual hardware is underway. As a future work, while the achieved selective model interpolation was observed to be effective for mechatronic applications, higher-order interpolation and potential trade-offs will be investigated. Briefly, these higher-order interpolation conditions can be translated to the core matrix equation analogously as the first-order derivative condition, and we expect the tools and knowledge from this paper will apply directly to extensional cases.

[2]The disturbance is a scaled analogy of actual disturbance in high precision motion system [2].

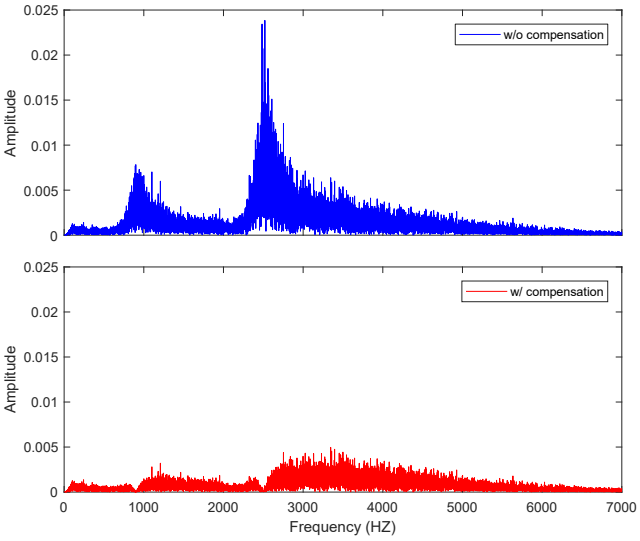

FIGURE 10. SPECTRUM COMPARISON WITH AND WITHOUT THE PROPOSED WIDE-BAND Q COMPENSATOR.

ACKNOWLEDGEMENT

T. J., J. T., and X. C. are grateful to support from the Department of Mechanical Engineering at the University of Connecticut. T. J. would like to acknowledge the partial financial support from the GE Fellowship for innovation.

REFERENCES

[1] Xu Chen and Masayoshi Tomizuka. A minimum parameter adaptive approach for rejecting multiple narrow-band disturbances with application to hard disk drives. *IEEE Transactions on Control System Technology*, 20(2):408 – 415, march 2012.

[2] Liting Sun, Tianyu Jiang, and Xu Chen. Adaptive loop shaping for wide-band disturbances attenuation in precision information storage systems. *IEEE Transactions on Magnetics*, 53(5):1–13, May 2017.

[3] J. Zheng and R.A. de Callafon. Recursive filter estimation for feedforward noise cancellation with acoustic coupling. *Journal of Sound and Vibration*, 291(3-5):1061–1079, April 2006.

[4] Jiawen Xu, Shilong Li, and Jiong Tang. Parametric analysis of piezoelectric metamaterial with lc shunt circuit. In *ASME 2016 Conference on Smart Materials, Adaptive Structures and Intelligent Systems*, volume 1, page V001T01A010, Stowe, Vermont, USA, September 2016.

[5] R M Ehrlich, J Adler, and H Hindi. Rejecting oscillatory, non-synchronous mechanical disturbances in hard disk drives. *IEEE Transactions on Magnetics*, 37(2):646–650, March 2001.

[6] Jinchuan Zheng, Guoxiao Guo, Youyi Wang, and Wai Ee Wong. Optimal Narrow-Band Disturbance Filter for PZT-Actuated Head Positioning Control on a Spinstand. *IEEE Transactions on Magnetics*, 42(11):3745–3751, 2006.

[7] Maarten Steinbuch. Repetitive control for systems with uncertain period-time. *Automatica*, 38(12):2103–2109, 2002.

[8] Cuiyan Li, Dongchun Zhang, and Xianyi Zhuang. A survey of repetitive control. In *Proceedings of 2004 IEEE/RSJ International Conference on Intelligent Robots and Systems*, volume 2, pages 1160–1166, 2004.

[9] Levin Jason and Petros Ioannou. Multirate adaptive notch filter with an adaptive bandwidth controller for disk drives. In *American Control Conference*, pages 4407–4412. IEEE, June 2008.

[10] I D Landau, M Alma, J J Martinez, and G Buche. Adaptive Suppression of Multiple Time-Varying Unknown Vibrations Using an Inertial Actuator. *IEEE Transactions on Control Systems Technology*, 19(6):1327–1338, 2011.

[11] Qixing Zheng and M Tomizuka. A disturbance observer approach to detecting and rejecting narrow-band disturbances in hard disk drives. In *Proceedings of 2008 IEEE International Workshop on Advanced Motion Control*, pages 254–259. IEEE, 2008.

[12] Xu Chen and Masayoshi Tomizuka. Overview and new results in disturbance observer based adaptive vibration rejection with application to advanced manufacturing. *International Journal of Adaptive Control and Signal Processing*, 29(11):1459–1474, 2015.

[13] J.C. Doyle, B.A. Francis, and A.R. Tannenbaum. *Feedback control theory*. Courier Corporation, 2013.

[14] Xu Chen, Tianyu Jiang, and Masayoshi Tomizuka. Pseudo youla-kucera parameterization with control of the waterbed effect for local loop shaping. *Automatica*, 62:177–183, 2015.

[15] D Youla, J Bongiorno, and H Jabr. Modern Wiener–Hopf design of optimal controllers Part I: The single-input-output case. *IEEE Transactions on Automatic Control*, 21(1):3–13, February 1976.

[16] D Youla, H Jabr, and J Bongiorno. Modern Wiener-Hopf design of optimal controllers–Part II: The multivariable case. *IEEE Transactions on Automatic Control*, 21(3):319–338, June 1976.

[17] Xu Chen and Hui Xiao. Multirate forward-model disturbance observer for feedback regulation beyond nyquist frequency. *System & Control Letters*, 94:181–188, 2016.

[18] Tianyu Jiang, Hui Xiao, and Xu Chen. An inverse-free disturbance observer for adaptive narrow-band disturbance rejection with application to selective laser sintering. In *ASME 2017 Dynamic Systems and Control Conference*, volume 3, page V003T32A006, Tysons, Virginia, USA, October 2017.

[19] K Hirano, S Nishimura, and S Mitra. Design of Digital Notch Filters. *IEEE Transactions on Communications*, 22(7):964–970, July 1974.